ASM | mSphere

Check for updates

| Genomics and Proteomics | Research Article

Temporal regulation of metabolic processes in the marine diazotroph *Crocosphaera watsonii* WH8501

Julia M. Gauglitz,[1,2] Keisuke Inomura,[3] Wout Bittremieux,[2] Dawn M. Moran,[1] Matthew R. McIlvin,[1] Mak A. Saito[1]

AUTHOR AFFILIATIONS See affiliation list on p. 17.

Downloaded from https://journals.asm.org/journal/msphere on 06 November 2026 by 131.128.73.132.

ABSTRACT Marine diazotrophic cyanobacteria play a crucial role in oceanic nitrogen cycling, supporting primary production and ecosystem balance. *Crocosphaera watsonii* WH8501 exemplifies this capability by temporally separating photosynthesis and diazotrophy. To investigate the regulatory mechanisms underlying this process, we employed mass spectrometry-based proteomics in a high-resolution diel culturing experiment, revealing tightly coordinated protein abundance patterns. Unsupervised clustering of diel protein abundance profiles identified six groups of co-regulated proteins characterized by distinct temporal expression patterns and functional categories. Cluster 1 contained nitrogen fixation and amino acid biosynthesis proteins that peaked at night, while cluster 2 included glycogen metabolism and photosynthetic dark reaction proteins that were most abundant during the night and day-night transition, supporting carbon consumption and energy production. Clusters 3 and 4 were enriched in proteins involved in photosynthesis, cell division, and lipid synthesis, with maximal abundance around midday. Cluster 5 comprised peptide biosynthesis proteins that peaked later in the day and may facilitate nitrogenase complex formation. Cluster 6, expressed during the day-night transition, revealed coordinated nitrogenase assembly, with Fe–S cluster proteins preceding peak nitrogenase iron protein abundance, suggesting a temporally ordered sequence of enzyme maturation. Distinct temporal patterns in iron trafficking to heme and Fe–S cluster biosynthetic systems further indicated tightly regulated allocation of iron to metalloproteins across the diel cycle. Together, these results reveal the intricate temporal coordination that enables *Crocosphaera* to balance nitrogen fixation and photosynthesis within a single cell and underscore the central role of diel regulation in sustaining these globally important processes.

IMPORTANCE Marine diazotrophic cyanobacteria play an essential role in global nitrogen cycling and ocean productivity. In this study, we investigate the temporal regulation of *Crocosphaera watsonii* metabolism using high-resolution proteomics under diel culturing conditions. Our analysis resolves six distinct clusters of protein abundance patterns across the light/dark cycle, reflecting intricate coordination of nitrogen fixation, photosynthesis, carbon allocation, and iron homeostasis. Notably, we identify temporally ordered assembly of nitrogenase subunits, including precursory expression of Fe–S cluster proteins and indications of tightly controlled iron trafficking systems. These findings provide new mechanistic insight into how unicellular diazotrophs synchronize key metabolic processes under natural diel cycles.

KEYWORDS proteome, diazotrophy, oxygen management, *Crocosphaera*, cyanobacteria, diel cycle

Marine cyanobacteria are oxygenic photoautotrophs that are responsible for up to 50% of primary production in surface waters (1). In addition to their importance

Editor Barbara J. Campbell, Clemson University, Clemson, South Carolina, USA

Address correspondence to Mak A. Saito, msaito@whoi.edu, or Julia M. Gauglitz, Julia.Gauglitz@uantwerpen.be.

The authors declare no conflict of interest.

See the funding table on p. 17.

This article is dedicated to Frederica Valois.

Received 20 May 2026
Accepted 23 September 2026
Published 20 October 2026

Copyright © 2026 Gauglitz et al. This is an open-access article distributed under the terms of the Creative Commons Attribution 4.0 International license.

to carbon flux in microbial food webs, some species are diazotrophic, or able to fix atmospheric N_2 into a bioavailable form (2). While cyanobacterial diazotrophs, such as the filamentous non-heterocystous *Trichodesmium*, were long thought to be the primary source of nitrogen fixation, recent insights indicate a prominent role for unicellular marine cyanobacteria, such as *Crocosphaera watsonii* WH8501, which have been shown to substantially contribute to N_2 fixation in tropical and subtropical waters (3–6).

The dual role of a diazotrophic cyanobacterium brings with it specific challenges, as photosynthesis and nitrogen fixation have an incompatibility that may complicate occurrence in the same milieu at the same time. The key enzyme in nitrogen fixation, nitrogenase, relies on an anaerobic environment (7, 8) and will be inactivated by oxygen, which evolves from photosystem II during light-dependent carbon fixation. Therefore, most microorganisms have evolved to employ either spatial or temporal separation of diazotrophy and photosynthesis. *C. watsonii* WH8501 is able to perform both of these processes by employing temporal separation (9), and the metabolic shift between inorganic C fixation during the day and N_2 fixation at night has now been well established (10, 11).

The nitrogenase enzyme is encoded in the nif gene operon, which contains the three structural proteins of the nitrogenase complex (NifH, NifD, and NifK) and proteins involved in cofactor biosynthesis and enzyme assembly. Maturation of the nitrogenase enzyme is a multi-step process and does not occur until the MoFe components are translated. The mature dinitrogenase enzyme is assembled from the Fe protein [4Fe–4S] cluster, then the P cluster, and then the FeMo cofactor, which provides the substrate reduction site. NifW binds to apo-MoFe (without FeMo-co) and is thought to stabilize the protein (12). NifT is a conserved nif-associated protein whose molecular role remains unknown; however, evidence suggests that it is not required for normal nitrogenase activity (13). The nitrogenase iron-sulfur cluster protein NifU is involved in the assembly and stabilization of the Fe–S clusters in nitrogenase, and the proteins SufB, SufC, and SufD, closely related components of the SUF (sulfur formation) system, contribute to proper assembly, maintenance, and protection of iron-sulfur clusters in the cell (14, 15). While gene transcript studies in *C. watsonii* WH8501 have demonstrated a diel pattern whereby the *nif* gene operon transcript levels cycle together over the day/night cycle (16), presence does not guarantee active function, as the nitrogenase complex components also require several other proteins to achieve catalytic competency and form the active nitrogenase enzyme (17). Interestingly, not all of the functions of the proteins necessary for optimal nitrogenase function have been determined, despite the importance of nitrogen fixation for global biogeochemical cycles and agriculture.

Oxygen management mechanisms that may protect nitrogenase include changes to cell permeability (18–20), controlled redox-based conformational change of nitrogenase (21, 22), increased respiration (respiratory protection) (18, 23–25), and physical protection/maintenance of oxygen-sensitive proteins (22, 23, 26). During respiratory protection, the level of respiration can be so high that it has been predicted to substantially lower growth efficiency (25) and growth rate (27), but the average cost of respiratory protection for *Crocosphaera* may be decreased by colony formation and metabolism specialization (28). In some cyanobacteria, Ni-dependent hydrogenases can help mitigate oxidative stress by consuming excess hydrogen produced during nitrogen fixation, which might otherwise react with oxygen (29). Additional proteins that may participate in broader protective mechanisms that mitigate oxidative stress during nitrogen fixation are radical SAM enzymes, which play an essential role in the biosynthesis and maintenance of the nitrogenase enzyme and its cofactors (30). Specifically, radical SAM supports the assembly and repair of Fe–S clusters. Other prior analyses have postulated that hopanoid lipid synthesis may protect cells from O_2 by decreasing their permeability (19) and that multiple protection mechanisms are in operation simultaneously (18, 25), enabling *Crocosphaera's* unique physiological capabilities.

Downloaded from https://journals.asm.org/journal/msphere on 06 November 2026 by 131.128.73.132.

A number of behaviors discriminate *C. watsonii* WH8501 from other phototrophs and likely play a role in facilitating *Crocosphaera*'s adaptation and competition in the oligotrophic open ocean environment. *C. watsonii* has been shown to meet its physiological requirement for iron in part via the temporal separation of nitrogen fixation and photosynthesis, enabling it to recycle iron atoms between key components of these two separate metabolic processes (31). Furthermore, temporal separation is marked by the cessation of photosystem II activity during the dark phase of the diel cycle (32), and *C. watsonii* can fix nitrogen, even in the presence of nitrate (NO_3^-) (33), indicating an expanded role for nitrogen fixation in the oceans (34).

Cyanobacteria are known for their ability to exhibit circadian rhythms, which are driven by a circadian clock (35), via mechanisms such as the oscilloid model established in the model organism *Synechococcus elongatus* PCC 7942. The oscilloid model is based on a three-protein oscillator system called KaiABC, where gene expression is regulated by the phosphorylation state of the KaiABC protein complex, which is embedded in a network of input and output factors (36, 37). A robust clock model consists of the genes *kaiA*, *kaiB*, *kaiC*, *sasA*, *cikA*, and *rpaA* (38). The *cikA* gene codes for a bacteriophytochrome-like histidine kinase and plays a role in the input signaling of the clock by sensing light via the detection of quinones via its C-terminal pseudo-receiver domain (39), providing a link between cellular metabolism and the clock. Tetratricopeptide repeat (TPR) motifs are a key structural component of CikA and are known to play a crucial role in its function. These motifs enable CikA to interact with other components of the circadian clock, thereby facilitating the transmission of environmental signals to the clock machinery (40). The concentration and redox state of quinones, which are light-dependent, may act to entrain the rhythmicity of the circadian clock to environmental stimuli. RpaA acts as a master regulator of global gene expression controlled by the circadian clock (41). It is a member of a two-component regulatory system, activated by phosphorylation, and is regulated by CikA, a bacteriophytochrome, and an antagonistic histidine kinase—SasA (42). The latest investigations into circadian clocks in *S. elongatus* PCC 7942 have established an *in vitro* model (43) that demonstrates the key role of output factors in the functioning of the circadian clock.

Protein abundances of potential circadian clock input and output factors have not been reported for *C. watsonii* WH8501, although it exhibits diel cycling of transcripts, contains genes for the KaiABC protein complex, and has been shown to exhibit changes in DNA topology (11) consistent with the oscilloid model established in *S. elongatus* PCC 7942. Observational studies are required to help determine whether the oscilloid model is the key form of temporal regulation. Protein degradation and translation throughout the day are critical for maintaining a highly dynamic diel cycle, and the cellular controls on protein abundance from an axenic culture of *C. watsonii* are therefore of great interest. Diel gene expression experiments frequently capture several time points in the dark and light phases or make a binary comparison between the light phase and the dark phase (i.e., noon and midnight) (44, 45). In particular, we hypothesized that more frequent sampling, particularly at the transition from light to dark, may yield insights into the metabolic restructuring and respiratory protection mechanisms particular to this diazotrophic cyanobacterium.

Here, we present a high-resolution diel proteomic analysis of axenic *C. watsonii* WH8501. Using liquid chromatography tandem mass spectrometry (LC-MS/MS), we quantified protein abundance at 1–2 h intervals over a full diel cycle to capture fine-scale temporal dynamics in metabolic regulation. This data set was compared to a previous lower-resolution diel experiment under identical growth conditions (31), which allowed us to validate previously observed patterns and reveal additional layers of regulation detectable only at higher temporal resolution. Together, these analyses demonstrate a distinct temporal ordering of proteins involved in nitrogen fixation, clarify their coordination with photosynthetic and metabolic processes, and provide new insight into the circadian mechanisms that structure diel metabolism in this globally significant cyanobacterial diazotroph.

Downloaded from https://journals.asm.org/journal/msphere on 06 November 2026 by 131.128.73.132.

Downloaded from https://journals.asm.org/journal/msphere on 06 November 2026 by 131.128.73.132.

MATERIALS AND METHODS

Culture conditions

Crocosphaera watsonii WH8501 was originally isolated from the tropical/subtropical South Atlantic Ocean (44) and grows in waters between 26°C and 32°C (45). Here, *C. watsonii* WH8501 was cultivated axenically in a 20 L acid-cleaned, autoclaved borosilicate glass carboy with a cotton plug and spigot by the addition of 1 L of culture to 16 L of sterile-filtered SO medium prepared with oligotrophic Sargasso Sea seawater, with no added nitrogen source (44). Cells were held in suspension, and the culture was aerated by pumping sterile air onto the surface of the culture while the culture was slowly stirred with a stir bar. The culture was monitored daily for growth by flow cytometry on a live sample, and two aliquots were fixed with paraformaldehyde and archived. The culture was verified axenic by growth tests in LB medium and by epifluorescence microscopy (Carl Zeiss, Thornwood, NY, USA) and maintained at 27°C with a 14:10 day:night light cycle with light ramp up/down at dusk and dawn, mimicking conditions at Station ALOHA in a diel incubator (Percival). The light intensity ranged from 0 to 120 lum/ft^2 units.

We began the diel experiment when the culture reached a log phase of growth, and samples were collected every 1–2 h over a 25 h period (n = 16). Sampling time began at t = 0. Light phase is time points 0 (0), 1 (1.5 h), 2 (3 h), 3 (4.5 h), 12 (18.5 h), 13 (20.5 h), 14 (22.5 h), and 15 (24 h), and dark phase is time points 4 (5.5 h), 5 (6.5 h), 6 (8.5 h), 7 (10.5 h), 8 (12.5 h), 9 (14.5 h), 10 (15.5 h), and 11 (16.5 h). For ease of reference to time during the 24 h period, "night" refers to ~6.5–15.5 h, "interface" refers to ~15.5–18.5 and ~3–6.5 h, "early day" refers to ~18.5–20.5 h, and "late day" refers to ~1.5–4.5 h (as used in Table 1). Red lights were used to illuminate the work area to minimize the impact of external cues on cellular metabolism during opening and closing of the incubator. During dawn and dusk, the sampling was every hour to capture the transitions in protein abundances associated with the onset of nitrogen fixation and photosynthesis. Approximately 50 mL of culture was drained to flush the spigot, after which samples were collected at each time point. Subsamples were taken for cell counts (fixed with paraformaldehyde and run on a Guava easyCyte HT system) and nitrogen fixation rate measurements (acetylene reduction assay, below). Cell counts over the course of the experiment can be found in the supplemental material (Fig. S1). Samples were centrifuged at 12,428 rcf for 20 min at 4°C, and the cell pellet was transferred and microcentrifuged at 6,700 rcf for 8 min at 4°C, further decanted, and frozen at −80°C until further analysis.

Acetylene reduction assay

As a proxy for nitrogen fixation, the acetylene reduction assay was performed by injecting 2 mL of concentrated acetylene gas into the headspace of a sealed 60 mL

TABLE 1 Overview of temporal trends and associated functions by cluster

Cluster	Time of max protein abundance	Example systems	Example proteins
1	Night	Nitrogen fixation	NifH, NifD, NifK, NifU, NifJ
		Amino acid biosynthesis	Threonine synthase
2	Night/interface	Glycogen metabolic process	Glucose-1-phosphate adenylyltransferase, glycogen synthase
		Photosynthesis, dark reaction	Light-independent protochlorophyllide reductase subunit B
3	Early day	Photosynthesis	ATP synthase subunits α, β, δ, ε
		Carbon fixation	Carboxysome shell protein CcmK
4	Early/late day	Photosynthesis	Photosystem II
		Cellular division	MurA, MurE, MurF, Ddl
		Lipid biosynthesis	Squalene synthase
5	Late day	Peptide biosynthesis	Small ribosomal subunit protein uS7
			Ala/Ser/Val/Gly/Cys/Met/Lys—tRNA ligases
6	Interface	Oxidoreductase complex	NADH ubiquinone oxidoreductase
		Translation	uS19, S11, L5, S21, L12

Nalgene culture bottle containing 20 mL of the sampled culture located in the incubator. The culture was incubated for 1 h, after which the headspace was measured for the reduction product (ethylene) by gas chromatography on a Shimadzu GC-8A using hydrogen as carrier gas and calibrated to a 9.1 ppb ethylene standard. One or two samples were collected at time points 3–9 to confirm active nitrogen fixation (Fig. S2).

Protein digestion and global proteomic analysis

Proteins were analyzed by a data-dependent acquisition LC-MS/MS method. Proteins were extracted by a magnetic bead method (Sera-Mag SpeedBeads [GE Healthcare Life Sciences]) and trypsin digested using a modification of previously published methods (31, 46) as described in Gauglitz et al. (47). Protein abundance was quantified by a colorimetric BCA protein assay (Thermo Fisher), and peptide extract in 2% DMSO was quantified using a colorimetric assay at 750 nm (DC protein assay; Biorad). Peptides were acidified with 1% formic acid and brought to a final concentration of 0.1 µg/uL with an LC-MS grade buffer containing 98% water, 2% ACN, and 0.1% formic acid.

Acidified protein extracts were analyzed by LC-MS/MS using a Michrom Advance HPLC coupled to a Thermo Scientific Orbitrap Fusion mass spectrometer with a Michrom Advance CaptiveSpray source. Each sample (1 µg protein measured before tryptic digestion) was concentrated onto a trap column (0.2 × 10 mm, 5 µm particle size, 120 Å pore size, ReproSil-Gold, Dr. Maisch GmbH) and rinsed with 100 µL of 0.1% formic acid, 5% ACN, and 95% water before gradient elution through a reverse phase C18 column (0.1 × 250 mm, 3 µm particle size, 120 Å pore size, ReproSil-Gold, Dr. Maisch GmbH) at a flow rate of 0.25 µL/min. The chromatography consisted of a nonlinear 210 min gradient from 5% to 95% buffer B, where A was 0.1% aqueous formic acid and B was 0.1% formic acid in ACN (all solvents were Fisher Optima grade). The mass spectrometer was set to perform MS/MS on the top N ions (Thermo Fusion) using data-dependent settings (dynamic exclusion 15 s, excluding unassigned and singly charged ions). Ions were monitored over a range of *m/z* 380–1,580.

Data processing

Mass spectral data (16 raw files) were processed in Proteome Discoverer 1.4 using SEQUEST (version 1.4.1.14) and Scaffold 4.4.6 (Proteome Software). Peptide identifications were made by implementing experiment-wide grouping with binary peptide-protein weights, a 97.0% peptide threshold, and a 99.0% minimum protein threshold with two peptides minimum at a 1.6% protein false discovery rate (FDR) and 0.0% peptide FDR. Mass spectra were mapped to the *Crocosphaera watsonii* WH8501 proteome (version November 2008, as used in the diel analysis in Saito et al. [31] to facilitate comparison of results; 5,659 entries; File S1) using the following search parameters: 0.60 Da fragment tolerance; 10.0 ppm parent mass tolerance, fixed modification of +57 on C (carbamidomethyl), variable modification of +16 on M (oxidation), and 2 max missed cleavages. A total of 1,148 proteins were identified, which represents a genome coverage of 20%. Table S2 contains an index of the sample information and filenames to facilitate reuse.

All proteomics data are given as relative protein abundance based on normalized spectral counts using the normalized spectral count abundance factor method implemented in Scaffold 4.4.6 (Proteome Software). Fold changes between light and dark phases were calculated as follows: mean values were computed for the light phase and dark phase separately, while imputing zero values by half of the minimum measured abundance across all proteins. *P* values were calculated using the *t*-test based on all abundance values between the light phase and the dark phase, and the Benjamini-Hochberg procedure was used for multiple testing correction.

Downloaded from https://journals.asm.org/journal/msphere on 06 November 2026 by 131.128.73.132.

Protein clustering

Protein abundances across all time points were analyzed using agglomerative clustering. First, proteins for which no molecular weight was assigned were removed. Next, the protein abundances were standardized by removing the mean and scaling to unit variance for each individual protein. Finally, the standardized protein abundances were clustered by agglomerative clustering with Ward linkage and the Euclidean distance. The distance threshold was set to 30 after visual inspection of the dendrogram (Fig. 1A). Data processing employed Pandas (version 2.0.3) (49), NumPy (version 1.25.2) (50), SciPy (version 1.11.1) (51), and Scikit-Learn (version 1.3.0) (52) for scientific data processing, and matplotlib (version 3.7.2) (53) and Seaborn (version 0.12.2) (54) for data visualization. Jupyter notebooks (55) were used for exploratory data analysis.

Downloaded from https://journals.asm.org/journal/msphere on 06 November 2026 by 131.128.73.132.

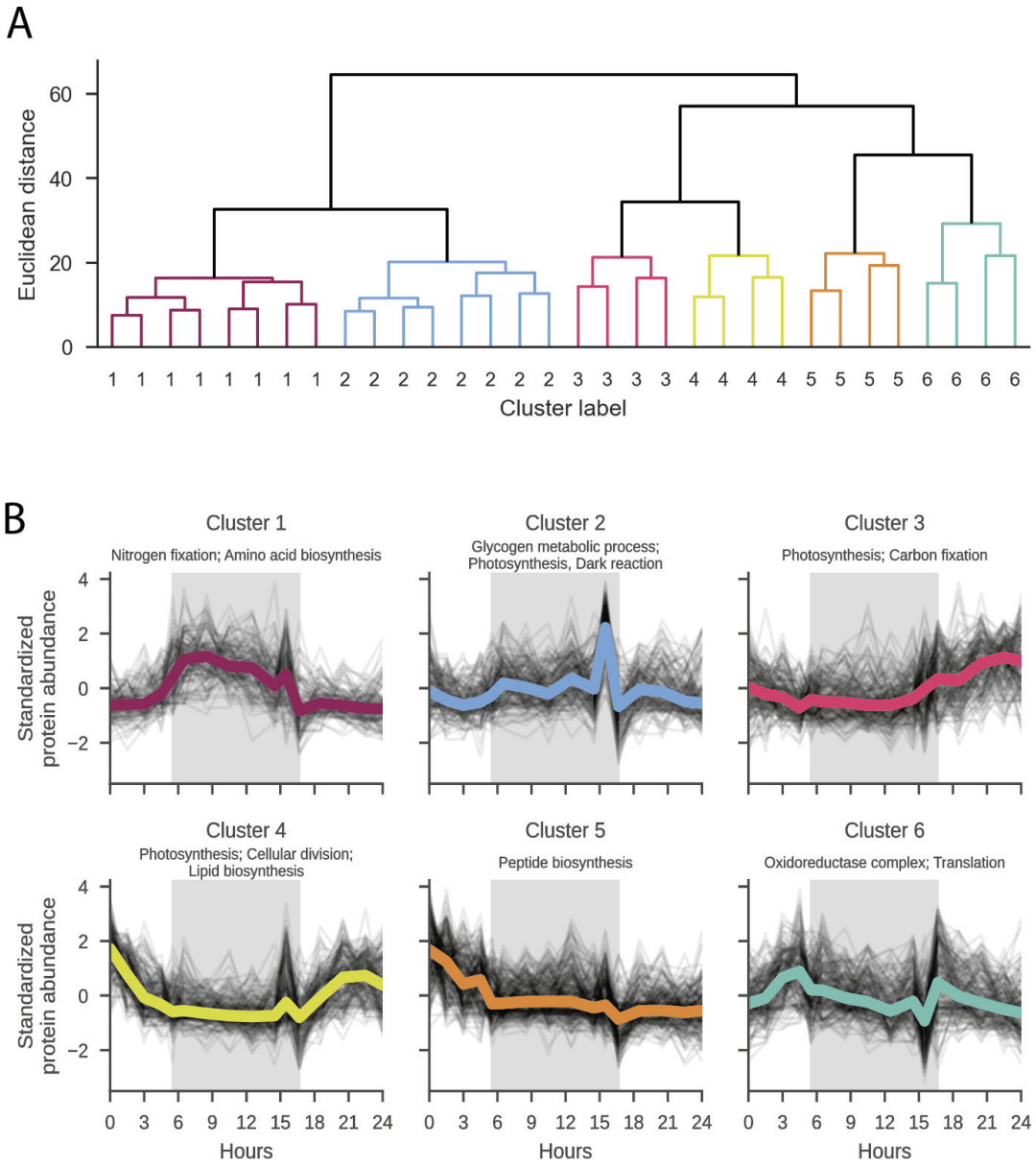

FIG 1 (A) Proteins clustered by agglomerative clustering with Ward linkage and the Euclidean distance. At a distance threshold of 30, there are six distinct clusters observed. Clusters 1 and 2 have the highest dissimilarity from clusters 3 through 6. (B) Standardized abundance of proteins grouped with each of the six data-driven clusters is plotted against hours. The dark phase is visualized by the gray background. Average abundance for all proteins in a cluster is colored by cluster as follows: cluster 1: magenta; cluster 2: blue; cluster 3: pink; cluster 4: yellow; cluster 5: orange; cluster 6: green.

Downloaded from https://journals.asm.org/journal/msphere on 06 November 2026 by 131.128.73.132.

GO analysis

Gene Ontology (GO) terms were used to annotate the *Crocosphaera watsonii* proteome because GO provides a detailed, hierarchical framework for describing biological processes, enabling clear discrimination among distinct energy-related pathways. This level of specificity is essential in cyanobacteria, where processes such as nitrogen fixation, carbon fixation, and photosynthetic energy generation must be analyzed separately to understand diel cellular physiology. In contrast, Clusters of Orthologous Genes categories group genes into coarse metabolic or functional classes (e.g., "energy production and conversion"), which do not differentiate between biologically distinct pathways, such as nitrogen fixation and carbon fixation, limiting their utility for process-level interpretation.

GO enrichment analysis for each cluster detected using agglomerative clustering was performed using the find_enrichment.py script from GOATOOLS (56). For each cluster, the protein identifiers for the proteins in that cluster were used as the study identifiers, all *C. watsonii* WH8501 protein identifiers read from the FASTA file were used as the population identifiers, and an association file mapping between Uniprot identifiers and GO terms retrieved from QuickGO (57) was used. Computed *P* values were corrected using the Benjamini-Hochberg procedure and thresholded at a *P* value of 0.05 after multiple hypothesis testing correction. Other configuration options were left at their default values. GO terms are hierarchical short phrases that describe the known biological function within the groups "biological process," "cellular compartment," and "molecular function." The max depth (MD) of GO terms refers to the depth within the hierarchy, with higher numbers indicating a more specialized role within the groups (File S3).

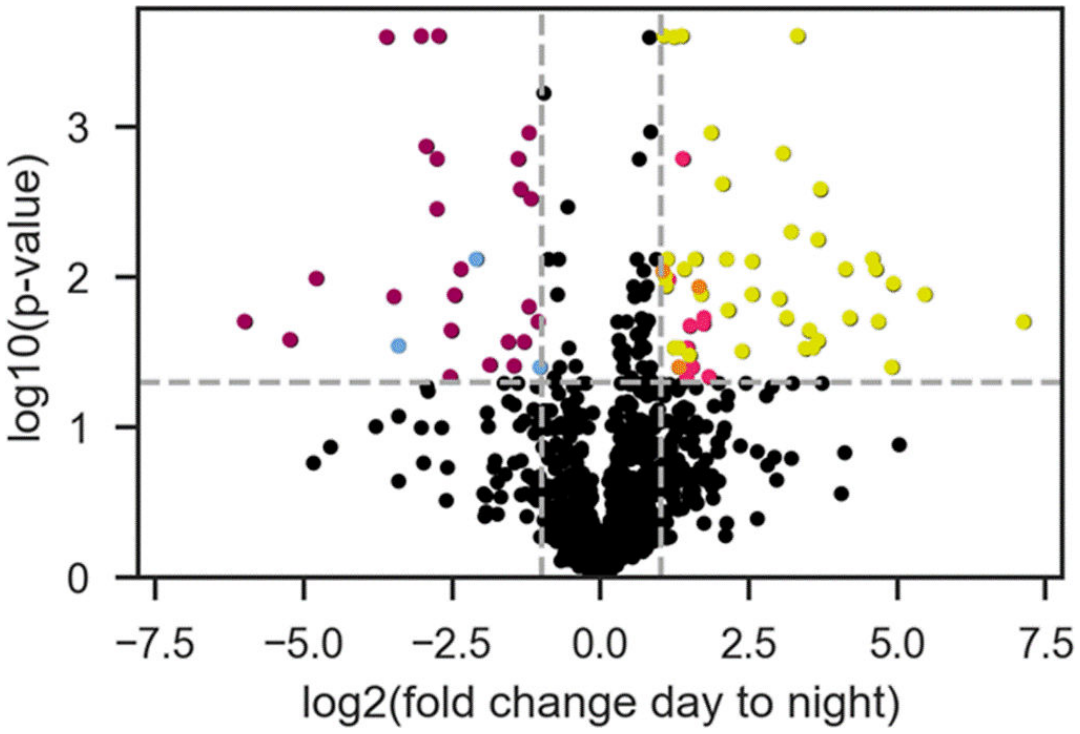

FIG 2 Volcano plot of the global proteome, showing the log2 fold change day to night vs the log10 of the *P* value. Twenty-seven proteins have statistically higher abundance in the dark period (upper left), while 51 proteins have statistically higher abundance during the light period (upper right). Proteins that are statistically significant and have a twofold or greater change in abundance (fold change of <−0.5 or >2; 218/1,148) are colored by cluster based on agglomerative clustering, as seen in Fig. 1 (cluster 1: magenta; cluster 2: blue; cluster 3: pink; cluster 4: yellow; and cluster 5: orange). No cluster six proteins meet the criteria, and thus green is not observed. Data can be found in Table S1.

The NIH tool protein BLAST (https://blast.ncbi.nlm.nih.gov/Blast.cgi) was used to search for additional protein identifications, particularly for proteins that were annotated as proteins of unknown function.

RESULTS

Diel proteome structure reveals six temporally regulated protein groups

Crocosphaera watsonii WH8501 expressed proteins with key roles in nitrogen fixation, photosynthesis, oxygen management, protein turnover, and putative circadian regulation, many of which varied systematically across the diel cycle. LC-MS/MS analysis identified 1,148 proteins, representing approximately 20% genome coverage. Agglomerative clustering of standardized protein abundances across the 16 sampled time points separated the diel proteome into six major clusters with distinct temporal profiles (Fig. 1). Clusters 1 and 2 were most abundant during the dark period or at the night/day interface, clusters 3 and 4 were most abundant during the light period, and clusters 5 and 6 were enriched near the light-dark transitions.

GO enrichment analysis supported the functional separation of these clusters. Cluster 1 was enriched for nitrogen fixation and related metabolic functions, whereas clusters 3 and 4 were enriched for photosynthesis, carbon fixation, cell division, and lipid-associated processes. Cluster 2 contained proteins associated with glycogen metabolism and light-independent photosynthetic reactions. Cluster 5 was enriched for proteins involved in peptide biosynthesis, and cluster 6 contained proteins associated with oxidoreductase complexes and translation (Table 1; File S3).

Light- and dark-phase comparisons identify proteins with strong diel abundance changes

Of the 1,148 proteins identified, 218 proteins showed at least a twofold difference in abundance between the light and dark phases. Among these, 78 proteins were both statistically significant and changed by at least twofold between photoperiods (Fig. 2; Table S1). Twenty-seven proteins were significantly more abundant during the dark period, whereas 51 proteins were significantly more abundant during the light period.

Proteins enriched during the light phase were primarily associated with photosynthesis, carbon metabolism, biosynthesis, and cell division. These included ketose-bisphosphate aldolase (Cwat3318), Photosystem II 12 kDa extrinsic protein (Cwat0626), S-layer homology region protein (Cwat6588), glycosyl transferases (Cwat0194, Cwat1204,

TABLE 2 *nif* gene products, their corresponding protein identity and/or role in nitrogen fixation and clustering pattern[a,b]

Gene	Identify and/or role of gene product	Cluster	Database ID	GO ID
nifE	Forms α2β2 tetramer with NifN. Required for FeMo-co synthesis. Proposed to function as a scaffold on which FeMo-co is synthesized	Cluster 1.1	CwatD3822	Q4C2Y4
nifN	Required for FeMo-co synthesis. Tetramer with NifE	Cluster 1.1	Cwat3823	Q4C2Y3
nifX	Involved in FeMo-co synthesis. Accumulates an FeSMo-containing precursor	Cluster 1.1	Cwat3824	Q4C2Y2
nifB	Required for FeMo-co synthesis. Its metabolic product, NifB-co, is a specific Fe and S donor to FeMo-co	Cluster 1.1	Cwat3815	Q4C2Z1
nifD	α subunit of MoFe protein. Forms an α2β2 tetramer with the β subunit. The site of substrate reduction, FeMo-co, is within the α subunit of MoFe protein	Cluster 1.2	Cwat3819	Q4C2Y7
nifK	β subunit of MoFe protein. P-clusters are present at each αβ subunit interface	Cluster 1.2	Cwat3820	Q4C2Y6
nifT	Unknown; evidence suggests that it is not required for normal nitrogenase activity	Cluster 1.2	Cwat3847	Q4C2Z7
nifJ	Pyruvate: flavodoxin (ferredoxin) oxidoreductase. Electron donor to Fe protein in *K. pneumoniae*	Cluster 1.2	Cwat1801	Q4BYB3
nifH	Fe protein. Obligate electron donor to MoFe protein during nitrogenase turnover. NifH is also required for FeMo-co biosynthesis and apo-MoFe protein maturation	Cluster 1.3	Cwat3818	Q4C2Y8
nifW	Involved in stability of MoFe protein	Cluster 1.3	Cwat3827	Q4C2X9
nifF	Flavodoxin. Physiological electron donor to NifH in *K. pneumoniae*	Cluster 1.3	Cwat4291	Q4C4V6
nifU	Molecular scaffold for the formation of Fe–S cluster for nitrogenase components	No cluster	Cwat3817	

[a]*nifH* and *nifU* gene products are observed during the entire diurnal cycle; all others become undetectable at one or more of the time points during the light phase. Table adapted from Rubio and Ludden (48).
[b]GO ID, UniProt ID.

Downloaded from https://journals.asm.org/journal/msphere on 06 November 2026 by 131.128.73.132.

Cwat3402, and Cwat3972), Entner-Doudoroff pathway protein (Cwat3088), and Calvin cycle protein (Cwat3318). Proteins involved in cell-wall synthesis and regulation of cell shape, including MurA (Cwat0821), MurE (Cwat3769), MurF (Cwat4119), and Ddl (Cwat4357), increased during the morning and peaked near midday, consistent with light-period cell division. MurA and Ddl also met the twofold and statistical significance criteria (cluster 4).

Temporally regulated translation of nitrogen fixation components

Proteins directly associated with nitrogen fixation were strongly enriched during the dark phase. These included NifH, NifD, NifK, NifW, NifU, and NifJ (Cwat3818, Cwat3819, Cwat3820, Cwat3827, Cwat3817, Cwat1801), as well as flavodoxin (Cwat4291) and heme oxygenase (Cwat2459) (Table 2). Additional dark-enriched proteins included NAD(P)(+)

Downloaded from https://journals.asm.org/journal/msphere on 06 November 2026 by 131.128.73.132.

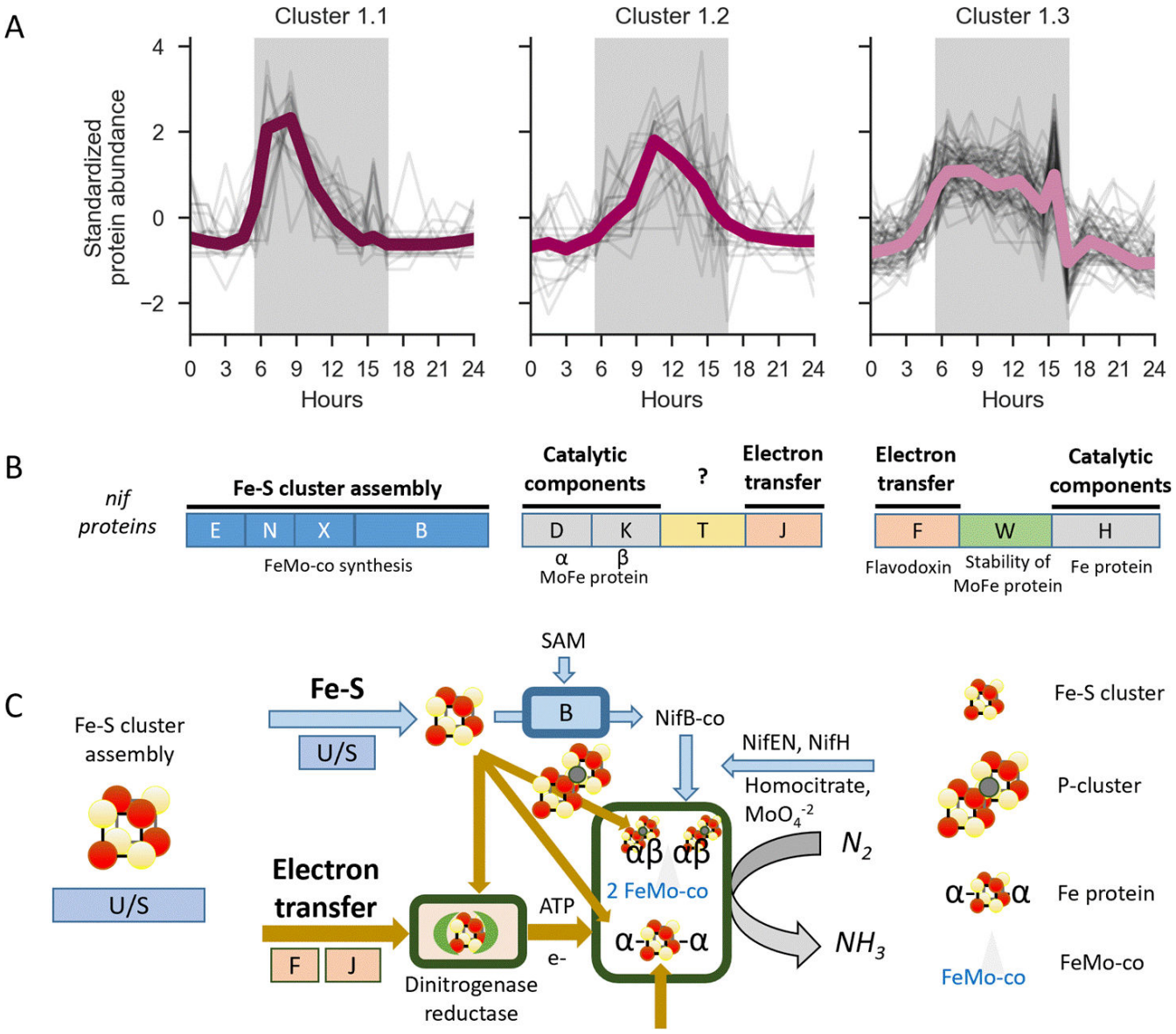

FIG 3 (A) Temporal progression of Nif biosynthetic groups. Standardized abundance of proteins grouped with cluster 1 sub-clusters during the diel cycle (cluster 1.4 not shown). The dark phase is visualized by the gray background. The average abundance for all proteins in a cluster is colored by cluster. (B) nif operon, genes, and colors align with the schema in part C and are labeled by their role (see also Table 2). The genes align with the clusters in A in which they are observed. (C) Schematic of the role and utilization of the different nitrogenase complex components in dinitrogen fixation. The abbreviations U, S, B, F, and J refer to the proteins from the respective *nif* genes. For example, B is the abbreviation for NifB.

transhydrogenase subunits and glucose-6-phosphate dehydrogenase, both of which can contribute to cellular reducing power by increasing NADPH availability. Proteins involved in amino acid biosynthesis and nitrogen assimilation, including threonine synthase (Cwat4050), 3-isopropylmalate dehydratase (Cwat1322), glutamate synthase (Cwat5417), RNA polymerase sigma factor SigA (Cwat5428), and chorismate synthase (Cwat2085), were also detected with dark-phase enrichment.

Nitrogen fixation was the most significantly enriched GO term in cluster 1 (adjusted *P* value of 3.85×10^{-14}). Further subclustering of cluster 1 resolved nitrogen-fixation-associated proteins into four temporal groups (Fig. 3), of which cluster 1.4 was not enriched in any terms and is not further discussed. Cluster 1.1 contained proteins associated with FeMo-cofactor biosynthesis, including NifE, NifN, NifX, and NifB. Cluster 1.2 contained the MoFe nitrogenase structural proteins NifD and NifK, along with NifT and NifJ. Cluster 1.3 contained NifH, NifW, and flavodoxin. NifU was detected throughout the diel cycle and was not assigned to these subclusters. These results confirmed the trends observed in Saito et al. (31), and due to the higher resolution of this data set, we were also able to identify further substructure in the abundance patterns of Nif proteins.

The temporal resolution of the experiment showed that NifB reached maximum abundance approximately 4 h before NifK (Fig. 4). NifH followed a profile similar to NifK, with lower abundance early in the dark period and maximum abundance after the midpoint of the night, coinciding with the period of maximum nitrogen fixation measured by acetylene reduction (16, 48) (Fig. S2). NifU abundance was higher during the night, and Suf proteins were most abundant in the first half of the night while remaining detectable throughout the diel cycle (31). These proteins facilitate the temporal regulation of Fe–S cluster assembly, stabilization, and maintenance.

Temporal signatures of oxygen management and nitrogenase protection

Several proteins associated with oxygen management, redox state, and potential nitrogenase protection showed temporal abundance patterns (Fig. 5). Squalene synthase (Cwat2696), a key enzyme in hopanoid biosynthesis, peaked near dusk. A Ni-dependent hydrogenase (Cwat0516) was detected at relatively high abundance, with a maximum

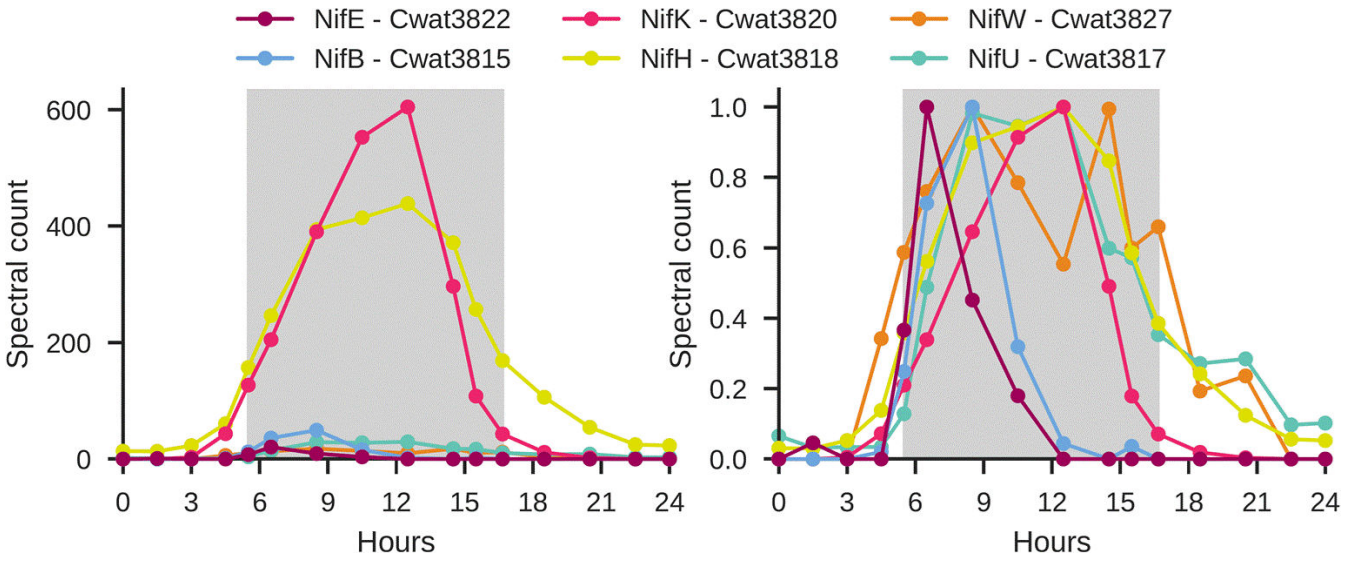

FIG 4 Temporal progression of Nif protein abundance. *Crocosphaera* NifB peak abundance is observed prior to NifH, indicating the production of Fe–S clusters prior to nitrogenase. MoFe cofactor biosynthesis protein NifE (Cwat3822—dark pink; cluster 1.1); nitrogen cofactor biosynthesis protein NifB (Cwat3815—blue; cluster 1.1); MoFe nitrogenase protein Beta chain—NifK (Cwat3820—pink; cluster 1.2); iron nitrogenase protein—NifH (Cwat3818—yellow; cluster 1.3); nitrogenase-stabilizing/protective protein NifW (Cwat3827—orange; cluster 1.3); nitrogenase iron-sulfur cluster protein NifU (Cwat3817—green; no cluster). Hours are relative to the start of the experiment, with the dark phase visualized by the gray background. Left: spectral counts. Right: spectral counts normalized to peak abundance per protein.

Downloaded from https://journals.asm.org/journal/msphere on 06 November 2026 by 131.128.73.132.

of 52 spectral counts, and showed diel entrainment. A putative Ni transport protein (Cwat4537), identified by BLAST analysis of proteins annotated as hypothetical, was detected only at dusk and peaked before the Ni-dependent hydrogenase.

Radical SAM (Cwat2761) also showed a transition-associated pattern, with highest abundance before or near the light-dark transition. Flavodoxin (Cwat4291), quinones, and several cytochrome c oxidases displayed distinct diel abundance profiles. These proteins included NADH-plastoquinone oxidoreductase chain 5 (Cwat4160), a putative methylase involved in ubiquinone/menaquinone biosynthesis (Cwat0228), NADH

Downloaded from https://journals.asm.org/journal/msphere on 06 November 2026 by 131.128.73.132.

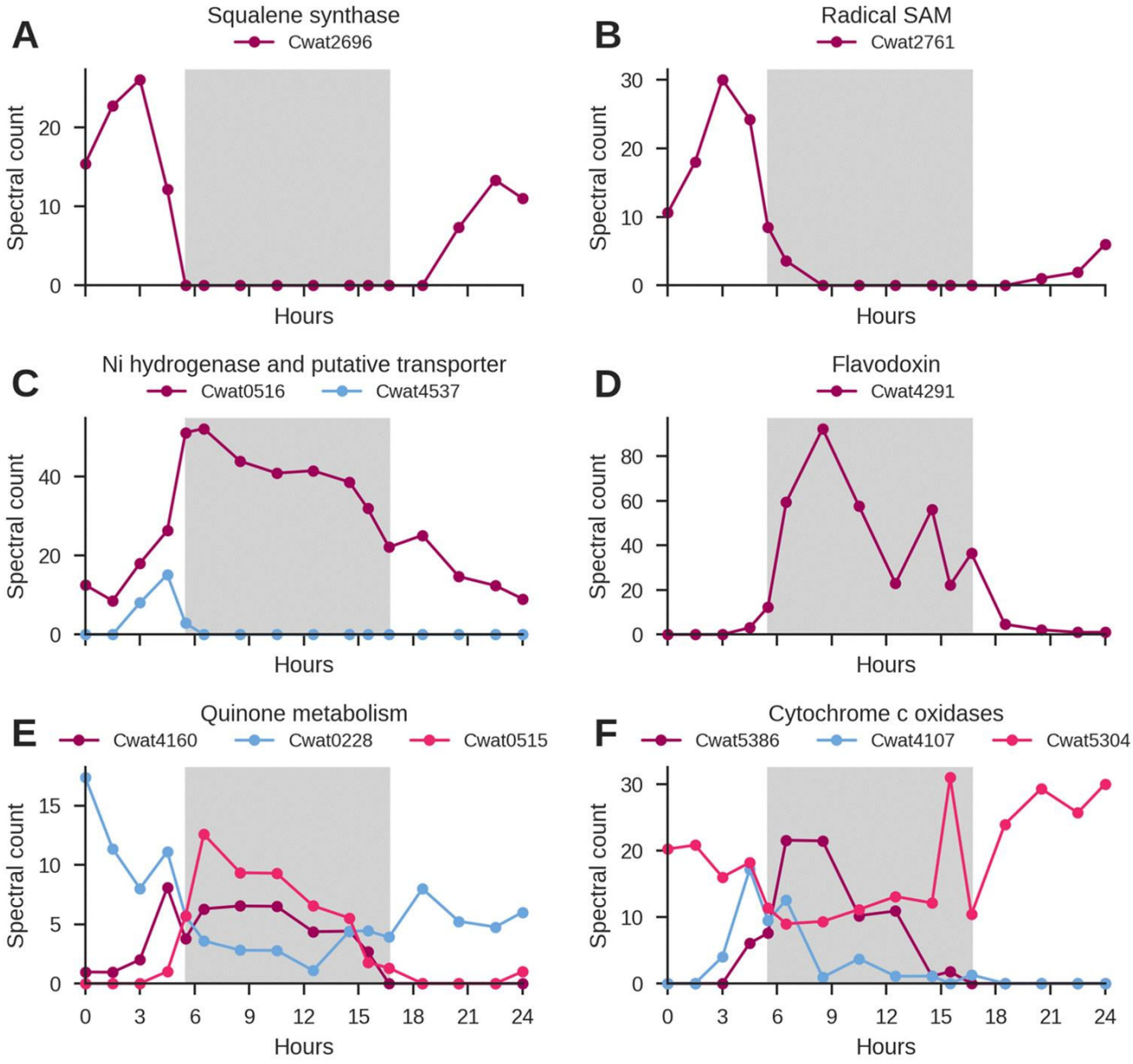

FIG 5 Temporal variability of selected proteins. (A) Squalene synthase (Cwat2696); (B) radical SAM (Cwat2761); (C) Ni hydrogenase (Q4BUZ7, Cwat0516; purple) and putative Ni transport protein (Cwat4537; blue); (D) flavodoxin (Q4C4V6, Cwat4291); (E) quinone metabolism (Cwat4160, NADH-plastoquinone oxidoreductase, chain 5, purple); (Cwat0228, similar to methylase involved in ubiquinone/menaquinone biosynthesis, blue); (Cwat0515, NADH ubiquinone oxidoreductase, 20 kDa subunit, (pink); (F) cytochrome c oxidases: (Cwat5386, purple); (Cwat4107, blue); (Cwat5304, pink). The dark phase is visualized by the gray background.

ubiquinone oxidoreductase 20 kDa subunit (Cwat0515), and cytochrome c oxidase proteins Cwat5386, Cwat4107, and Cwat5304.

Evidence of a circadian clock in *C. watsonii*

Circadian-clock-associated proteins KaiA (Cwat4942), KaiB (Cwat4943), KaiC (Cwat4944), and a second KaiC-like protein (Cwat5154) were detected; however, they did not show a clear diel abundance trend (Fig. S3). Homologs of sasA and ldpA were present in the genome based on BLAST alignment, but the corresponding proteins were not detected. No homologous proteins were identified for CikA, Pex, or CpmA in the genome used for this analysis.

Several proteins containing TPR motifs were observed with diel patterns, including proteins with higher abundance during the day in clusters 4 and 5. Putative LabA and LalA proteins, as well as RpaB (Cwat5773), were also detected but did not exhibit clear oscillating abundance patterns. A putative RpaA response regulator (Cwat6453), with 98.4% amino acid sequence identity to RpaA by BLASTp, showed a clear diel pattern and contributed to GO enrichment in cluster 4 (Fig. 6A).

Cluster 6 showed marked abundance changes near dawn and dusk and was enriched for the GO term "oxidoreductase complex." A hypothetical protein identified by BLASTp as having oxidoreductase activity and a FAD/NAD binding domain (Cwat2868) was most abundant at the light-dark transition (Fig. 6). Quinone-associated proteins also showed temporal changes, including proteins whose abundance shifted around the transitions between light and dark.

Protein turnover and translation machinery are temporally structured

Protein degradation and translation machinery also showed diel organization. Across the proteome, 49 proteins representing 28 distinct peptidase annotations were identified (Table 3). These peptidases included serine peptidases, metallopeptidases, endopeptidases, signal peptide cleavage peptidases, carboxypeptidases, and enzymes involved in peptidoglycan remodeling (Fig. 6). Peptidases associated with peptidoglycan remodeling were distributed across all six clusters. D-Ala-D-Ala carboxypeptidase C (peptidase S13; Cwat4934), for example, was most abundant during the day (Fig. 6C). Signal peptide cleavage peptidases were most abundant during the day and at the light-dark interface (Fig. 6D).

Four ClpP proteins were detected throughout the diel cycle, but their abundance profiles differed. Two ClpP proteins peaked early in the day, one peaked during both early and late days, and one was most abundant late in the day (Fig. 6E, Table 3). Ribosomal proteins involved in translation also increased in abundance before the dark period and peaked as the lights were ramped down. These included uS19, S11, L5, S21, L12, and uS2, as well as a YbaB/EbfC family nucleoid-associated protein (Cwat2370), which contributed to enrichment of the GO term "intracellular non-membrane-bounded organelle" in cluster 6.

Additional temporal signatures: light-independent photosynthetic reactions, glycogen metabolism, and metal cofactor biosynthesis

Other light-independent processes were captured by clusters 1 and 2. Photosystem II (Cwat3258) was significantly more abundant in the dark than in the light, consistent with previous diel observations (31). Cluster 2 was enriched for the GO term "photosynthesis, dark reaction" through proteins, including light-independent protochlorophyllide reductase subunit B (chlB; Cwat0967), ribulose bisphosphate carboxylase large chain (cbbL/RuBisCO; Cwat2714), light-independent protochlorophyllide reductase iron-sulfur ATP-binding protein (Cwat4016), and light-independent protochlorophyllide reductase subunit N (chlN; Cwat4018).

The GO term "glycogen (starch) synthase activity" was also observed. Starch synthase (Cwat6377), however, did not show strong diel variability in this experiment. Clusters 1 and 2 were additionally enriched for metal-binding and metal-cluster-binding terms,

Downloaded from https://journals.asm.org/journal/msphere on 06 November 2026 by 131.128.73.132.

including 4Fe–4S cluster binding and iron-sulfur cluster binding. Proteins with oxidoreductase activity were enriched in both clusters: "CH–CH group of donors" with NAD or NADP as acceptor in cluster 2 and hydrogen, aldehyde, or oxo, and iron-sulfur proteins as donors with iron-sulfur protein and dinitrogen as acceptors in cluster 1. Three vitamin biosynthesis proteins (thiamine, riboflavin, and cobalamin), a copper-translocating ATPase, and ferrochelatase (Cwat3000) reached maximum abundance at temporal interfaces (Fig. 6). Ferrochelatase displayed a large peak near dusk and a smaller peak near dawn.

DISCUSSION

C. watsonii WH8501 reorganizes a substantial fraction of its detected proteome over a single diel cycle. The six protein clusters provide a framework for understanding how

Downloaded from https://journals.asm.org/journal/msphere on 06 November 2026 by 131.128.73.132.

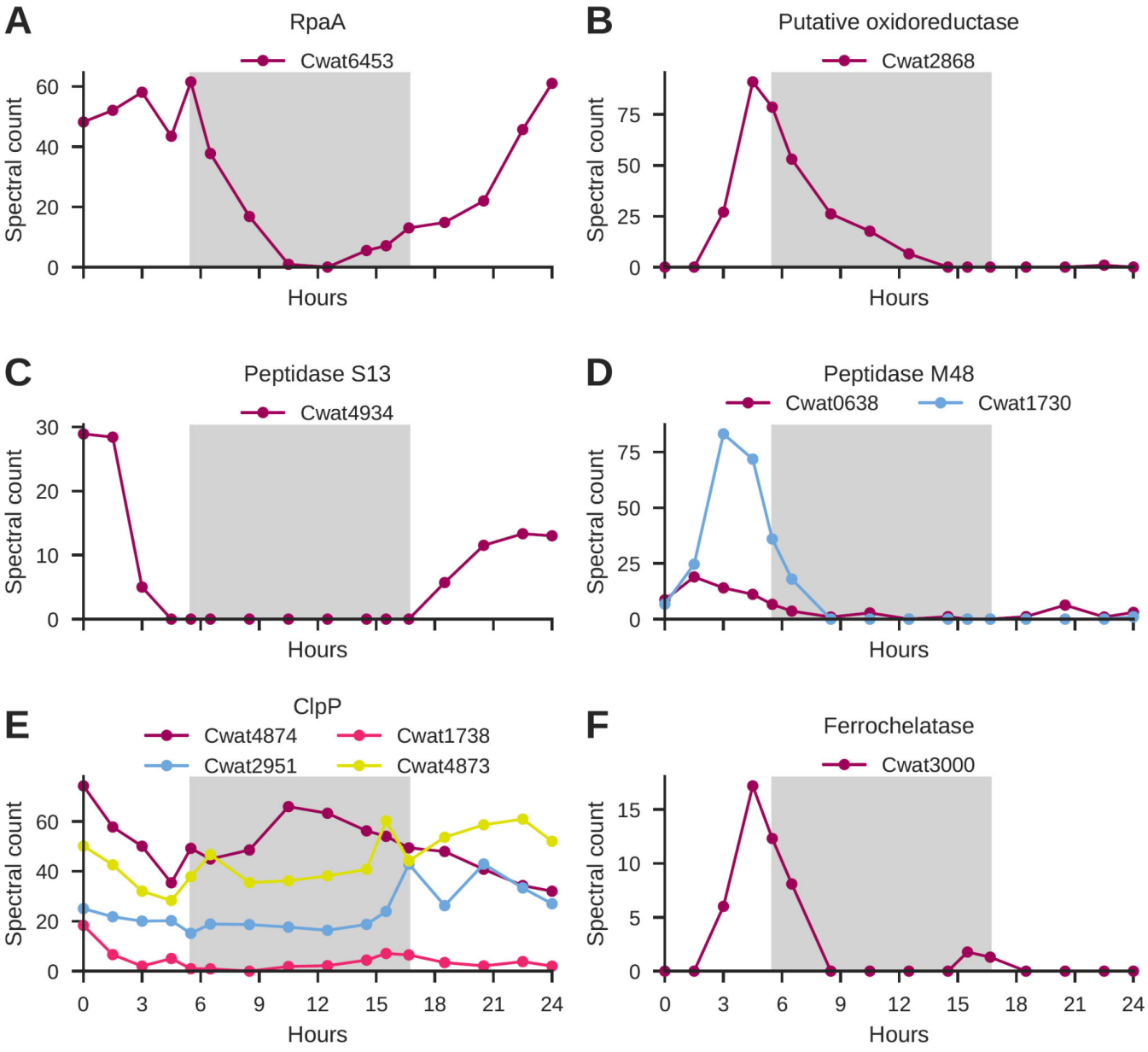

FIG 6 Temporal variability of selected proteins. (A) Abundance of proteins RpaA (response regulator receiver: transcriptional regulatory protein, C-terminal; Cwat6453; Q4C9J3); (B) the putative oxidoreductase Cwat2868 (oxidoreductase activity; FAD/NAD binding domain); (C) peptidase S13 (Cwat4934); (D) peptidase M48 (Cwat0638 and Cwat1730); (E) ClpP, peptidase S14 (Cwat4874, Cwat1738, Cwat2951, Cwat4873); and (F) ferrochelatase (Cwat3000).

TABLE 3 Peptidases organized by cleavage type, cluster number, and the time of maximum protein abundance for each cluster[a]

Cleavage type	Peptidase(s) in indicated cluster (time of max protein abundance per cluster)					
	1 (night)	2 (night/interface)	3 (early day)	4 (early/late day)	5 (late day)	6 (interface)
Aminopeptidase		LAP		M1		
Carboxypeptidase		M20D		M20D		
C-terminal processing				S41A(2)		S41A
Endopeptidase	M61		M16, M41	M41, OpdA	M41 (3)	M16 (3)
General protein processing			ClpP (2)	ClpP	ClpP, S8/S53	S1
Peptidoglycan remodeling	M22	M50 (2)	M23B (2)	S13, family 51	S51, M15B/M15C	S13, M52
Proline-specific cleavage				S49	S9, POP	
Regulation of DNA gyrase activity	U62			U62 (2)	U62	
Signal peptide cleavage			S24	SPI (2)	M48	M48
Unknown				Unspecified (1)		Unspecified (1)

[a]Peptidases are labeled by their abbreviation in the M or S categorization, corresponding to a metallopeptidase or a serine peptidase, as applicable. A key to CwatDRAFT numbers can be found in File S2. Other abbreviations used: POP, prolyl oligopeptidase; OpdA, oligopeptidase A; LAP, leucyl aminopeptidase; SPI, signal peptidase I; ClpP, peptidase S14; GT51, glycosyltransferases in family 51.

Downloaded from https://journals.asm.org/journal/msphere on 06 November 2026 by 131.128.73.132.

this unicellular cyanobacterium coordinates photosynthesis, nitrogen fixation, carbon storage, protein turnover, and cofactor biosynthesis across light and dark phases. The day-enriched clusters were dominated by photosynthesis, cell division, and biosynthetic functions, whereas the night-enriched clusters contained nitrogen fixation, redox metabolism, and iron-sulfur-related proteins. This organization is consistent with the established temporal separation of photosynthesis and nitrogen fixation in *C. watsonii* (10, 31), but the higher sampling frequency reveals additional ordering within these broad day/night programs. Importantly, the overall agreement with the diel proteomic patterns reported by Saito et al. (31) demonstrates that these metabolic transitions are highly reproducible under controlled laboratory conditions, while the increased sampling frequency allows finer-scale temporal structure within those transitions to be resolved.

Nitrogenase abundance patterns suggest ordered assembly rather than uniform nif expression, as nitrogen-fixation proteins do not simply rise and fall as a single group. Instead, the higher-resolution data set resolves a sequence in which proteins associated with FeMo-cofactor biosynthesis peak before the structural MoFe nitrogenase components, followed by NifH, NifW, and flavodoxin. This pattern is consistent with the biochemical requirements of nitrogenase maturation: cofactor assembly must precede the formation of a catalytically competent nitrogenase complex. Similar to results from *Azotobacter vinelandii* (58), production of cofactor (nifB) does not require the presence of the nitrogenase protein, and the observation that NifB peaks several hours before NifK supports the interpretation that *C. watsonii* prepares metal cofactors before the major catalytic components reach maximum abundance.

This ordering may also reflect the physiological constraints imposed by oxygen sensitivity. Nitrogenase activity must occur after photosynthetic oxygen production has declined, but delaying all nitrogenase-related protein synthesis until the cell is fully dark-adapted would constrain the window for nitrogen fixation. A temporally staged assembly process may allow the cell to prepare cofactor and scaffold components before full nitrogenase activity begins, while limiting the exposure of the more oxygen-sensitive iron-sulfur clusters.

The persistence of NifU and NifH outside the main dark-phase peak is also notable. NifU may be retained to support rapid iron-sulfur cluster formation, whereas NifH has roles beyond electron donation during nitrogenase turnover, including FeMo-cofactor biosynthesis and apo-MoFe maturation. Alternatively, residual detection during the light period may partly reflect incomplete degradation or differential protein stability.

Oxygen management appears multifactorial and temporally coordinated. The high-resolution proteomic data support a model in which *C. watsonii* uses multiple overlapping strategies to protect nitrogenase from oxygen exposure. Squalene synthase, Ni-dependent hydrogenase, cytochrome c oxidases, radical SAM enzymes, flavodoxin,

and quinone-associated proteins each showed diel or transition-associated abundance patterns. Although the primary function of cytochromes is electron transport, we postulate that the increased abundance of cytochromes (Cwat4107, Cwat5386; Fig. 5F) reflects enhanced respiratory activity, which could contribute to respiratory protection by accelerating oxygen consumption around the cell while simultaneously increasing ATP availability to support energy-intensive processes such as nitrogen fixation. These observations are consistent with several non-exclusive respiratory protection mechanisms: reduced membrane permeability through hopanoid-associated pathways, increased respiratory oxygen consumption, redox balancing, and maintenance or repair of oxygen-sensitive Fe–S proteins (30, 59, 60), as also postulated in modeling studies (18, 28, 61).

The temporal ordering of these proteins is important. Squalene synthase and a putative Ni transporter peaked around dusk, before or near the onset of nighttime nitrogen fixation. Radical SAM and quinone-associated proteins also changed near the light-dark transition. These patterns suggest that the cell begins preparing the intracellular environment for nitrogenase function before peak nitrogen fixation occurs.

Protein turnover is likely central to diel restructuring. The breadth of peptidases and ClpP proteins detected across the diel cycle indicates that protein degradation is an important component of temporal regulation in *C. watsonii*. Because nitrogenase, photosynthetic complexes, redox proteins, and cell-division proteins must be remodeled daily, proteolysis likely works together with transcription and translation to shape the observed abundance profiles. In *Synechococcus elongatus* PCC 7942, Clp proteins contribute to proteome remodeling, which is essential for circadian clock function (62). The temporal distribution of ClpP proteins and signal-peptide-processing enzymes in *C. watsonii* suggests that protein turnover and maturation are not constant background processes but are themselves diel-regulated.

The data also raise an important mechanistic question: how selectively does *C. watsonii* degrade nitrogenase components after the dark period? Some proteins, such as NifU and NifH, remain detectable beyond the main nighttime nitrogen-fixation window, whereas other nitrogenase-associated proteins become undetectable during parts of the light phase. This could reflect selective protease activity, differences in protein stability, functional retention of specific components, or limitations in detection.

Temporal coordination of metal and cofactor allocation may be a key organizing principle. The enrichment of iron-sulfur-cluster-binding proteins, metal-binding proteins, ferrochelatase, vitamin biosynthesis enzymes, and copper-associated transport machinery at specific diel phases suggests that metal and cofactor allocation is tightly coordinated with the metabolic cycle. This is particularly relevant for *C. watsonii* because photosynthesis and nitrogen fixation both impose high demands for metalloproteins, especially iron-containing proteins. For example, ferrochelatase (Cwat3000) catalyzes the insertion of iron into protoporphyrin IX to form heme, a critical cofactor for cytochromes that supports photosynthetic electron transport proteins, including respiratory proteins like cytochrome c oxidase at dusk and cytochrome b6f at dawn, consistent with the distinct large and small peaks observed in ferrochelatase. The temporally ordered abundance of ferrochelatase, nitrogenase Fe–S, and FeMo-cofactor-related proteins suggests that the cell coordinates heme and iron-sulfur biosynthesis with the transition from photosynthetic to diazotrophic metabolism.

This interpretation also connects the proteomic results to the ecological constraints experienced by marine diazotrophs. In oligotrophic environments, efficient metal use and recycling may be essential for sustaining both photosynthesis and nitrogen fixation. The diel separation of these pathways may therefore reduce direct competition for metal cofactors while allowing the same cell to perform both processes over a 24-h cycle, as discussed in Saito et al. (31).

Downloaded from https://journals.asm.org/journal/msphere on 06 November 2026 by 131.128.73.132.

Broader implications and limitations

These results provide a high-resolution view of how *C. watsonii* WH8501 coordinates diel metabolism at the protein level. The data support a model in which daytime photosynthesis, carbon fixation, cell division, and biosynthetic processes are followed by a transition period marked by redox remodeling, protein translation, cofactor preparation, and oxygen-management proteins. This transition precedes the nighttime accumulation of nitrogenase-associated proteins and measured nitrogen-fixation activity. The temporal ordering of Nif proteins suggests that nitrogenase maturation is not governed solely by uniform nif operon expression but instead involves staged accumulation of cofactor biosynthesis proteins, MoFe nitrogenase components, electron-transfer proteins, and stabilizing factors.

This temporal structure has broader implications for understanding how unicellular oxygenic diazotrophs maintain incompatible metabolic processes within a single cell. The observed timing of ferrochelatase, Fe–S cluster-related proteins, oxidoreductases, hydrogenase, quinone-associated proteins, and peptidases suggests that metal trafficking, redox state, and protein turnover are central components of this daily metabolic reorganization.

Several limitations should be considered. Protein abundance does not necessarily indicate enzyme activity, complex assembly, or post-translational regulatory state. This is particularly important for nitrogenase and the Kai circadian system, where catalytic activity, phosphorylation, and protein-protein interactions may be more informative than total protein abundance alone. For example, the redox state of the cell may indeed play an important role in both entraining circadian rhythms and enabling a favorable environment for nitrogen fixation (59, 60). The detection of KaiA, KaiB, and KaiC proteins confirms that core circadian-clock components are present in the proteome, but their abundance did not oscillate strongly. This result is expected for a Kai-based oscillator, where timing is often encoded through phosphorylation state, protein-protein interactions, and output signaling rather than large changes in total Kai protein abundance (35). Because this study did not measure phosphorylation, the lack of Kai abundance oscillation should not be interpreted as evidence against a functional circadian clock.

Instead, the more informative signals may lie in putative input and output factors. RpaA showed a clear diel pattern, as also observed in Saito et al. (31), and cluster 6 contained proteins with transition-associated oxidoreductase activity. Quinone-associated proteins also changed across the diel cycle. Together, these observations are consistent with a model in which cellular redox state and metabolic transitions help entrain or transmit circadian signals. In addition, inferred oxygen-protection mechanisms will require direct physiological validation.

Together, these findings validate and extend previous diel proteomic studies of *C. watsonii* by confirming major day-night metabolic patterns while resolving fine-scale temporal transitions that were not detectable at lower sampling resolution. They provide a framework for interpreting diel field proteomes, where sampling time can strongly influence the apparent abundance of nitrogen-fixation, photosynthetic, redox-associated, and metal-binding proteins. The collection of protein data sets in the field can then, in turn, contribute to accurately capturing potential new nitrogen due to nitrogen fixation in global biogeochemical models, which will be increasingly more important given the shifting and likely expanding range of growth for nitrogen fixers such as *C. watsonii*.

ACKNOWLEDGMENTS

We would like to thank the National Science Foundation for the NSF OCE PRF awarded to J.M.G. (1421196). This work was supported by a grant from the Simons Foundation (LS-ECIAMEE-00001549, K.I.), NSF OCE 2227425 to K.I. and 2123055, 2125063, and

Downloaded from https://journals.asm.org/journal/msphere on 06 November 2026 by 131.128.73.132.

2048774 to M.A.S., NIH R01GM135709, and the Center for Chemical Currencies on a Microbial Planet (NSF 2019589).

Very special thanks go to John B. Waterbury for insightful discussions and mentorship and Frederica Valois for her support, scientific guidance, and assistance in the lab.

AUTHOR AFFILIATIONS

[1]Marine Chemistry and Geochemistry Department, Woods Hole Oceanographic Institution (WHOI), Woods Hole, Massachusetts, USA
[2]Department of Computer Science, University of Antwerp, Antwerp, Belgium
[3]Graduate School of Oceanography, University of Rhode Island, Narragansett, Rhode Island, USA

PRESENT ADDRESS

Julia M. Gauglitz, Department of Computer Science, University of Antwerp, Antwerp, Belgium

AUTHOR ORCIDs

Julia M. Gauglitz http://orcid.org/0000-0003-3146-2489
Wout Bittremieux http://orcid.org/0000-0002-3105-1359
Mak A. Saito http://orcid.org/0000-0001-6040-9295

FUNDING

Funder	Grant(s)	Author(s)
National Science Foundation	1421196	Julia M. Gauglitz
Simons Foundation		Keisuke Inomura
National Science Foundation	2227425	Keisuke Inomura
National Science Foundation	2123055, 2125063, 2048774, 2019589	Mak A. Saito
National Institutes of Health	R01GM135709	Mak A. Saito

AUTHOR CONTRIBUTIONS

Julia M. Gauglitz, Conceptualization, Formal analysis, Funding acquisition, Investigation, Methodology, Supervision, Visualization, Writing – original draft, Writing – review and editing | Keisuke Inomura, Funding acquisition, Writing – original draft, Writing – review and editing | Wout Bittremieux, Formal analysis, Visualization, Writing – original draft, Writing – review and editing | Dawn M. Moran, Methodology | Matthew R. McIlvin, Investigation, Methodology | Mak A. Saito, Conceptualization, Funding acquisition, Supervision, Writing – review and editing

DATA AVAILABILITY

The mass spectrometry proteomics data have been deposited to the ProteomeXchange Consortium via the PRIDE (63) partner repository with the data set identifier PXD072247. Processed data are available in the supplemental material. All code and analysis notebooks to generate the figures and analyses presented in this paper are freely available on GitHub at https://github.com/jgauglitz/Croco_diel under the open-source Apache 2.0 license.

ADDITIONAL FILES

The following material is available online.

Downloaded from https://journals.asm.org/journal/msphere on 06 November 2026 by 131.128.73.132.

Supplemental Material

File S1 (mSphere00324-26-s0001.txt). Crocosphaera proteins.
File S2 (mSphere00324-26-s0002.xlsx). Spectral count data.
File S3 (mSphere00324-26-s0003.xlsx). GO data by cluster.
Fig. S1 (mSphere00324-26-s0004.png). Cell growth.
Fig. S2 (mSphere00324-26-s0005.png). Nitrogen fixation.
Fig. S3 (mSphere00324-26-s0006.png). KaiABC proteins.
Legends (mSphere00324-26-s0007.pdf). Supplemental material legends.
Table S1 (mSphere00324-26-s0008.csv). Significant proteins between day and night.
Table S2 (mSphere00324-26-s0009.xlsx). Index samples.

Downloaded from https://journals.asm.org/journal/msphere on 06 November 2026 by 131.128.73.132.

REFERENCES

1. Chisholm SW, Olson RJ, Zettler ER, Goericke R, Waterbury JB, Welschmeyer NA. 1988. A novel free-living prochlorophyte abundant in the oceanic euphotic zone. Nature 334:340–343. https://doi.org/10.1038/334340a0
2. Bergman B, Gallon JR, Rai AN, Stal LJ. 1997. N2 fixation by non-heterocystous cyanobacteria. FEMS Microbiol Rev 19:139–185. https://doi.org/10.1016/S0168-6445(96)00028-9
3. Montoya JP, Holl CM, Zehr JP, Hansen A, Villareal TA, Capone DG. 2004. High rates of N2 fixation by unicellular diazotrophs in the oligotrophic Pacific Ocean. Nature 430:1027–1032. https://doi.org/10.1038/nature02824
4. Falcón LI, Carpenter EJ, Cipriano F, Bergman B, Capone DG. 2004. N2 fixation by unicellular bacterioplankton from the Atlantic and Pacific oceans: phylogeny and *in situ* rates. Appl Environ Microbiol 70:765–770. https://doi.org/10.1128/AEM.70.2.765-770.2004
5. Zehr JP, Waterbury JB, Turner PJ, Montoya JP, Omoregie E, Steward GF, Hansen A, Karl DM. 2001. Unicellular cyanobacteria fix N2 in the subtropical North Pacific Ocean. Nature 412:635–638. https://doi.org/10.1038/35088063
6. Zehr JP, Mellon MT, Zani S. 1998. New nitrogen-fixing microorganisms detected in oligotrophic oceans by amplification of nitrogenase (nifH) genes. Appl Environ Microbiol 64:3444–3450. https://doi.org/10.1128/AEM.64.9.3444-3450.1998
7. Fay P. 1992. Oxygen relations of nitrogen fixation in cyanobacteria. Microbiol Rev 56:340–373. https://doi.org/10.1128/mr.56.2.340-373.1992
8. Gallon JR. 1992. Reconciling the incompatible: N2 fixation and O2. New Phytol 122:571–609. https://doi.org/10.1111/j.1469-8137.1992.tb00087.x
9. Berman-Frank I, Quigg A, Finkel ZV, Irwin AJ, Haramaty L. 2007. Nitrogen - fixation strategies and Fe requirements in cyanobacteria. Limnol Oceanogr 52:2260–2269. https://doi.org/10.4319/lo.2007.52.5.2260
10. Shi T, Ilikchyan I, Rabouille S, Zehr JP. 2010. Genome-wide analysis of diel gene expression in the unicellular N(2)-fixing cyanobacterium *Crocosphaera watsonii* WH 8501. ISME J 4:621–632. https://doi.org/10.1038/ismej.2009.148
11. Pennebaker K, Mackey KRM, Smith RM, Williams SB, Zehr JP. 2010. Diel cycling of DNA staining and nifH gene regulation in the unicellular cyanobacterium *Crocosphaera watsonii* strain WH 8501 (Cyanophyta). Environ Microbiol 12:1001–1010. https://doi.org/10.1111/j.1462-2920.2010.02144.x
12. Van Stappen C, Jiménez-Vicente E, Pérez-González A, Yang Z-Y, Seefeldt LC, DeBeer S, Dean DR, Decamps L. 2022. A conformational role for NifW in the maturation of molybdenum nitrogenase P-cluster. Chem Sci 13:3489–3500. https://doi.org/10.1039/d1sc06418e
13. Nonaka A, Yamamoto H, Kamiya N, Kotani H, Yamakawa H, Tsujimoto R, Fujita Y. 2019. Accessory proteins of the nitrogenase assembly, NifW, NifX/NafY, and NifZ, are essential for diazotrophic growth in the nonheterocystous cyanobacterium *Leptolyngbya boryana*. Front Microbiol 10:495. https://doi.org/10.3389/fmicb.2019.00495
14. Dos Santos PC, Smith AD, Frazzon J, Cash VL, Johnson MK, Dean DR. 2004. Iron-sulfur cluster assembly. J Biol Chem 279:19705–19711. https://doi.org/10.1074/jbc.M400278200
15. Wollers S, Layer G, Garcia-Serres R, Signor L, Clemancey M, Latour J-M, Fontecave M, Ollagnier de Choudens S. 2010. Iron-sulfur (Fe-S) cluster assembly. J Biol Chem 285:23331–23341. https://doi.org/10.1074/jbc.M110.127449
16. Mohr W, Intermaggio MP, LaRoche J. 2010. Diel rhythm of nitrogen and carbon metabolism in the unicellular, diazotrophic cyanobacterium *Crocosphaera watsonii* WH8501. Environ Microbiol 12:412–421. https://doi.org/10.1111/j.1462-2920.2009.02078.x
17. Dos Santos PC, Fang Z, Mason SW, Setubal JC, Dixon R. 2012. Distribution of nitrogen fixation and nitrogenase-like sequences amongst microbial genomes. BMC Genomics 13:162. https://doi.org/10.1186/1471-2164-13-162
18. Inomura K, Deutsch C, Wilson ST, Masuda T, Lawrenz E, Lenka B, Sobotka R, Gauglitz JM, Saito MA, Prášil O, Follows MJ. 2019. Quantifying oxygen management and temperature and light dependencies of nitrogen fixation by *Crocosphaera watsonii*. mSphere 4:e00531-19. https://doi.org/10.1128/mSphere.00531-19
19. Cornejo-Castillo FM, Zehr JP. 2019. Hopanoid lipids may facilitate aerobic nitrogen fixation in the ocean. Proc Natl Acad Sci USA 116:18269–18271. https://doi.org/10.1073/pnas.1908165116
20. Sabra W, Zeng A-P, Deckwer W-D. 2001. Bacterial alginate: physiology, product quality and process aspects. Appl Microbiol Biotechnol 56:315–325. https://doi.org/10.1007/s002530100699
21. Rutledge HL, Rittle J, Williamson LM, Xu WA, Gagnon DM, Tezcan FA. 2019. Redox-dependent metastability of the nitrogenase P-cluster. J Am Chem Soc 141:10091–10098. https://doi.org/10.1021/jacs.9b04555
22. Schlesier J, Rohde M, Gerhardt S, Einsle O. 2016. A conformational switch triggers nitrogenase protection from oxygen damage by shethna protein II (FeSII). J Am Chem Soc 138:239–247. https://doi.org/10.1021/jacs.5b10341
23. Poole RK, Hill S. 1997. Respiratory protection of nitrogenase activity in *Azotobacter vinelandii*--roles of the terminal oxidases. Biosci Rep 17:303–317. https://doi.org/10.1023/a:1027336712748
24. Oelze J. 2000. Respiratory protection of nitrogenase in *Azotobacter* species: is a widely held hypothesis unequivocally supported by experimental evidence? FEMS Microbiol Rev 24:321–333. https://doi.org/10.1111/j.1574-6976.2000.tb00545.x
25. Inomura K, Bragg J, Follows MJ. 2017. A quantitative analysis of the direct and indirect costs of nitrogen fixation: a model based on *Azotobacter vinelandii*. ISME J 11:166–175. https://doi.org/10.1038/ismej.2016.97
26. Robson RL, Postgate JR. 1980. Oxygen and hydrogen in biological nitrogen fixation. Annu Rev Microbiol 34:183–207. https://doi.org/10.1146/annurev.mi.34.100180.001151
27. Inomura K, Wilson ST, Deutsch C. 2019. Mechanistic model for the coexistence of nitrogen fixation and photosynthesis in marine *Trichodesmium*. mSystems 4:e00210-19. https://doi.org/10.1128/mSystems.00210-19
28. Masuda T, Inomura K, Takahata N, Shiozaki T, Sano Y, Deutsch C, Prášil O, Furuya K. 2020. Heterogeneous nitrogen fixation rates confer energetic advantage and expanded ecological niche of unicellular diazotroph populations. Commun Biol 3:172. https://doi.org/10.1038/s42003-020-0894-4
29. Tuit C, Waterbury J, Ravizza G. 2004. Diel variation of molybdenum and iron in marine diazotrophic cyanobacteria. Limnol Oceanogr 49:978–990. https://doi.org/10.4319/lo.2004.49.4.0978
30. Liu YA, Quechol R, Solomon JB, Lee CC, Ribbe MW, Hu Y, Hedman B, Hodgson KO. 2022. Radical SAM-dependent formation of a nitrogenase cofactor core on NifB. J Inorg Biochem 233:111837. https://doi.org/10.1016/j.jinorgbio.2022.111837

Downloaded from https://journals.asm.org/journal/msphere on 06 November 2026 by 131.128.73.132.

31. Saito MA, Bertrand EM, Dutkiewicz S, Bulygin VV, Moran DM, Monteiro FM, Follows MJ, Valois FW, Waterbury JB. 2011. Iron conservation by reduction of metalloenzyme inventories in the marine diazotroph *Crocosphaera watsonii*. Proc Natl Acad Sci USA 108:2184–2189. https://doi.org/10.1073/pnas.1006943108
32. Rabouille S, Claquin P. 2016. Photosystem-II shutdown evolved with nitrogen fixation in the unicellular diazotroph *Crocosphaera watsonii*. Environ Microbiol 18:477–485. https://doi.org/10.1111/1462-2920.13157
33. Großkopf T, Laroche J. 2012. Direct and indirect costs of dinitrogen fixation in *Crocosphaera watsonii* WH8501 and possible implications for the nitrogen cycle. Front Microbiol 3:236. https://doi.org/10.3389/fmicb.2012.00236
34. Rabouille S, Randall B, Talec A, Raimbault P, Blasco T, Latifi A, Oschlies A. 2021. Independence of a marine unicellular diazotroph to the presence of NO_3^-. Microorganisms 9:2073. https://doi.org/10.3390/microorganisms9102073
35. Schmelling NM, Lehmann R, Chaudhury P, Beck C, Albers S-V, Axmann IM, Wiegard A. 2017. Minimal tool set for a prokaryotic circadian clock. BMC Evol Biol 17:169. https://doi.org/10.1186/s12862-017-0999-7
36. Mori T, Johnson CH. 2001. Circadian programming in cyanobacteria. Semin Cell Dev Biol 12:271–278. https://doi.org/10.1006/scdb.2001.0254
37. Fang M, LiWang A, Golden SS, Partch CL. 2024. The inner workings of an ancient biological clock. Trends Biochem Sci 49:236–246. https://doi.org/10.1016/j.tibs.2023.12.007
38. Chavan AG, Swan JA, Heisler J, Sancar C, Ernst DC, Fang M, Palacios JG, Spangler RK, Bagshaw CR, Tripathi S, Crosby P, Golden SS, Partch CL, LiWang A. 2021. Reconstitution of an intact clock reveals mechanisms of circadian timekeeping. Science 374:eabd4453. https://doi.org/10.1126/science.abd4453
39. Ivleva NB, Gao T, LiWang AC, Golden SS. 2006. Quinone sensing by the circadian input kinase of the cyanobacterial circadian clock. Proc Natl Acad Sci USA 103:17468–17473. https://doi.org/10.1073/pnas.0606639103
40. Schmitz O, Katayama M, Williams SB, Kondo T, Golden SS. 2000. CikA, a bacteriophytochrome that resets the cyanobacterial circadian clock. Science 289:765–768. https://doi.org/10.1126/science.289.5480.765
41. Markson JS, Piechura JR, Puszynska AM, O'Shea EK. 2013. Circadian control of global gene expression by the cyanobacterial master regulator RpaA. Cell 155:1396–1408. https://doi.org/10.1016/j.cell.2013.11.005
42. Gutu A, O'Shea EK. 2013. Two antagonistic clock-regulated histidine kinases time the activation of circadian gene expression. Mol Cell 50:288–294. https://doi.org/10.1016/j.molcel.2013.02.022
43. Fang M, Chavan AG, LiWang A, Golden SS. 2023. Synchronization of the circadian clock to the environment tracked in real time. Proc Natl Acad Sci USA 120:e2221453120. https://doi.org/10.1073/pnas.2221453120
44. Waterbury JB, Willey JM. 1988. Isolation and growth of marine planktonic cyanobacteria, p 100–105. *In* Methods in enzymology; cyanobacteria. Vol. 167. Academic Press.
45. Webb EA, Ehrenreich IM, Brown SL, Valois FW, Waterbury JB. 2009. Phenotypic and genotypic characterization of multiple strains of the diazotrophic cyanobacterium, *Crocosphaera watsonii*, isolated from the open ocean. Environ Microbiol 11:338–348. https://doi.org/10.1111/j.1462-2920.2008.01771.x
46. Hughes CS, Foehr S, Garfield DA, Furlong EE, Steinmetz LM, Krijgsveld J. 2014. Ultrasensitive proteome analysis using paramagnetic bead technology. Mol Syst Biol 10:757. https://doi.org/10.15252/msb.20145625
47. Gauglitz JM, Boiteau RM, McLean C, Babcock-Adams L, McIlvin MR, Moran DM, Repeta DJ, Saito MA. 2021. Dynamic proteome response of a marine *Vibrio* to a gradient of iron and ferrioxamine bioavailability. Mar Chem 229:103913. https://doi.org/10.1016/j.marchem.2020.103913
48. Rubio LM, Ludden PW. 2005. Maturation of nitrogenase: a biochemical puzzle. J Bacteriol 187:405–414. https://doi.org/10.1128/JB.187.2.405-414.2005
49. McKinney W. 2010. Data structures for statistical computing in Python. Python in Science Conference; Austin, TX: , p 56–61. https://doi.org/10.25080/Majora-92bf1922-00a
50. Harris CR, Millman KJ, van der Walt SJ, Gommers R, Virtanen P, Cournapeau D, Wieser E, Taylor J, Berg S, Smith NJ, et al. 2020. Array programming with NumPy. Nature 585:357–362. https://doi.org/10.1038/s41586-020-2649-2
51. Virtanen P, Gommers R, Oliphant TE, Haberland M, Reddy T, Cournapeau D, Burovski E, Peterson P, Weckesser W, Bright J, et al. 2020. SciPy 1.0: fundamental algorithms for scientific computing in Python. Nat Methods 17:261–272. https://doi.org/10.1038/s41592-019-0686-2
52. Pedregosa F, Varoquaux G, Gramfort A, Michel V, Thirion B, Grisel O, Blondel M, Prettenhofer P, Weiss R, Dubourg V, Vanderplas J, Passos A, Cournapeau D, Brucher M, Perrot M, Duchesnay É. 2011. Scikit-learn: machine learning in Python. J Mach Learn Res 12:2825–2830.
53. Hunter JD. 2007. Matplotlib: a 2D graphics environment. Comput Sci Eng 9:90–95. https://doi.org/10.1109/MCSE.2007.55
54. Waskom M. 2021. Seaborn: statistical data visualization. JOSS 6:3021. https://doi.org/10.21105/joss.03021
55. Kluyver T, Ragan-Kelley B, Pé Rez F, Granger B, Bussonnier M, Kelley K, Hamrick J. 2016. Jupyter notebooks – a publishing format for reproducible computational workflows, p 87–90. *In* Positioning and power in academic publishing: players, agents and agendas. IOS Press.
56. Klopfenstein DV, Zhang L, Pedersen BS, Ramírez F, Warwick Vesztrocy A, Naldi A, Mungall CJ, Yunes JM, Botvinnik O, Weigel M, Dampier W, Dessimoz C, Flick P, Tang H. 2018. GOATOOLS: a Python library for gene ontology analyses. Sci Rep 8:10872. https://doi.org/10.1038/s41598-018-28948-z
57. Binns D, Dimmer E, Huntley R, Barrell D, O'Donovan C, Apweiler R. 2009. QuickGO: a web-based tool for gene ontology searching. Bioinformatics 25:3045–3046. https://doi.org/10.1093/bioinformatics/btp536
58. Dixon R, Kahn D. 2004. Genetic regulation of biological nitrogen fixation. Nat Rev Microbiol 2:621–631. https://doi.org/10.1038/nrmicro954
59. Berman-Frank I, Lundgren P, Falkowski P. 2003. Nitrogen fixation and photosynthetic oxygen evolution in cyanobacteria. Res Microbiol 154:157–164. https://doi.org/10.1016/S0923-2508(03)00029-9
60. Kim Y-I, Vinyard DJ, Ananyev GM, Dismukes GC, Golden SS. 2012. Oxidized quinones signal onset of darkness directly to the cyanobacterial circadian oscillator. Proc Natl Acad Sci USA 109:17765–17769. https://doi.org/10.1073/pnas.1216401109
61. Inomura K, Deutsch C, Masuda T, Prášil O, Follows MJ. 2020. Quantitative models of nitrogen-fixing organisms. Comput Struct Biotechnol J 18:3905–3924. https://doi.org/10.1016/j.csbj.2020.11.022
62. Cohen SE, McKnight BM, Golden SS. 2018. Roles for ClpXP in regulating the circadian clock in *Synechococcus elongatus*. Proc Natl Acad Sci USA 115:E7805–E7813. https://doi.org/10.1073/pnas.1800828115
63. Perez-Riverol Y, Bandla C, Kundu DJ, Kamatchinathan S, Bai J, Hewapathirana S, John NS, Prakash A, Walzer M, Wang S, Vizcaíno JA. 2025. The PRIDE database at 20 years: 2025 update. Nucleic Acids Res 53:D543–D553. https://doi.org/10.1093/nar/gkae1011